Available online at www.eccomasproceedia.org
Eccomas Proceedia COMPDYN (2017) 1732-1747

ECCOMAS
Proceedia

COMPDYN 2017
6th ECCOMAS Thematic Conference on
Computational Methods in Structural Dynamics and Earthquake Engineering
M. Papadrakakis, M. Fragiadakis (eds.)
Rhodes Island, Greece, 15–17 June 2017

RINTC PROJECT: NONLINEAR ANALYSES OF ITALIAN CODE-CONFORMING BASE-ISOLATED BUILDINGS FOR RISK OF COLLAPSE ASSESSMENT

D. Cardone[1], N. Conte[1], A. Dall'Asta[2], A. Di Cesare[1], A. Flora[1], G. Leccese[1], A. Mossucca[1], F. Micozzi[2], C. Ponzo[1], L. Ragni[3]

[1] University of Basilicata – School of Engineering
Viale dell'Ateneo Lucano 10 - Potenza
e-mail: donatello.cardone@unibas.it,nadiaconte91@gmail.com,antodice@yahoo.it, amedeo.flora85@gmail.com,gianmarco.leccese@unibas.it,an.mossucca@yahoo.it,felice.ponzo@unibas.it,

[2] University of Camerino – School of Architecture and Design
Piazza Cavour 19/f - Camerino
e-mail: andrea.dallasta@unicam.it,fabio.micozzi@unicam.it

[3] Polytechnic University of Marche – Department of Construction, Civil engineering and Architecture. Via Brecce Bianche - Ancona
e-mail: laura.ragni@univpm.it

Keywords: Base isolation, Friction pendulum systems, Rubber bearings, Nonlinear dynamic analysis, Multi-stripe analyses, Risk assessment

Abstract. *This paper reports on the results of an ongoing Research Project aimed at computing the risk of collapse of new buildings conforming to the Italian Seismic Design Code. Companion papers describe the overall Research Project, funded by the Italian Civil Protection Department (DPC), its different areas of application (reinforced concrete, masonry, steel buildings, etc), the overall seismic risk calculation procedure and the ground motion selection process followed to identify the recorded ground motions used for the multi-stripe analyses for twenty different ground motion intensities. This paper describes the nonlinear analyses on a number of reinforced concrete (RC) buildings equipped with different isolation systems. Base isolation is one of the most widespread techniques currently used for seismic protection of buildings and their equipment. The present study presents the results for a six storey RC building isolated with different base seismic isolation systems based on: (i) rubber bearings; (ii) rubber bearings and flat sliding bearings; (iii) friction pendulum systems. The isolation systems have been designed according to current Italian seismic code considering different suitable combinations of stiffness and damping or friction. The failure conditions of the proposed isolation systems and peak responses of building have been evaluated through nonlinear dynamic analysis performed under bidirectional ground motions, considering twenty couple of natural earthquakes for ten different peak ground accelerations. The results point out that all isolation systems work effectively in limiting the building damage for seismic intensities much higher than the design earthquake. On the other hand, they have a little margin to collapse beyond the design seismic intensity.*

Peer-review under responsibility of the organizing committee of COMPDYN 2017.
doi: 10.7712/120117.5525.19365

1 INTRODUCTION

Base isolation is one of the most widespread techniques currently used for seismic protection of buildings and their equipment. This paper describes the nonlinear analyses on a new reinforced concrete (RC) building equipped with different isolation systems conforming to the Italian Seismic Design Code [1] aimed at computing the risk of collapse and the risk of damage of the nonstructural components. In particular, eight different case studies of base isolated buildings located in L'Aquila (soil type C) have been considered in this study: two cases present an isolation system composed only by High Damping Rubber Bearings (HDRBs), four cases present an hybrid isolation system composed by HDRBs and Steel-PTFE sliders and the other two cases present a friction pendulum (FPS) isolation system. Such cases differ only for the dimensional and mechanical properties of the isolation system while featuring the same prototype building with similar dimensions and reinforcements of structural elements. Specifically, the superstructure of the isolated building prototype analyzed in the present study derives from the six-storey fixed base RC frame buildings considered by the WP of the research project working on RC structures [2]. The building is intended for residential use and it is characterized by a regular plan of approximately 240 square meters and 6 stories above ground. The height of the ground level is 3.4m while that of all the other stories is equal to 3.05m. The building structure includes the staircase, designed with knee beams. All floor plans are identical; the only differences are in the column and beam dimensions and reinforcement. The minimum column size is 35 cm. Figure 1a shows the typical structural plan, where the fixed reference grid is highlighted and the arrows indicate the orientation of the one way slabs (with thickness of 25cm). The outer beams are all deep, while all internal beams are flat, as shown in Figure 1b.The 3D frame included infill panels modelled for design and analysis purposes, as reported in Figure 2a, whereas Figure 2b reports the elastic response spectra for the site and the soil considered.

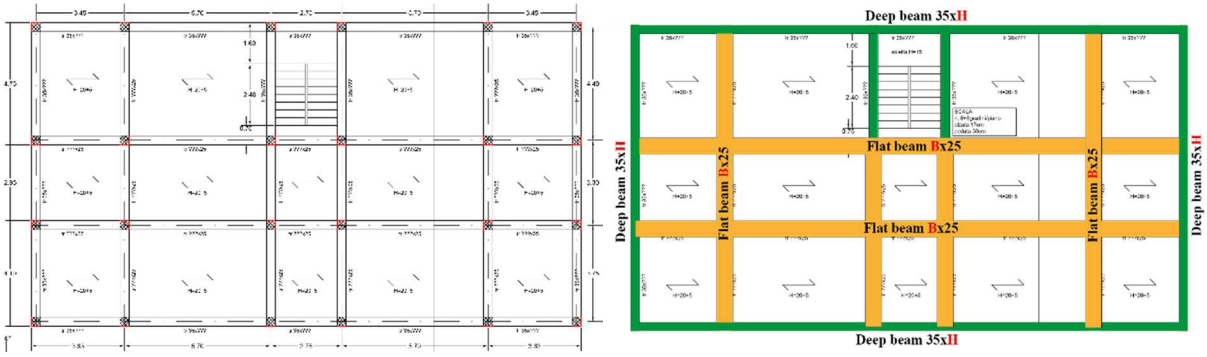

(a) (b)

Figure 1: a) floor plan with fixed reference grid and b) beam types

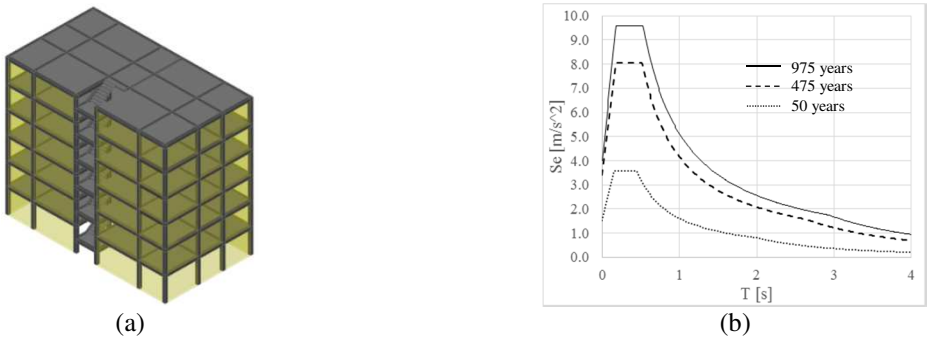

(a) (b)

Figure 2: a) 6-story infill frame and b) horizontal elastic response spectra for different return periods (b)

2 DESIGN OF THE STUDY CASES

The seismic design of the isolated buildings has been performed by means of a modal response spectrum analysis, following the indications of the Italian NTC 2008[1] design code. In this section, a summary of the structural design is reported, for both the isolation system and the superstructure.

2.1 Isolation system

For the two study cases presenting an isolation system composed only by HDRBs, due to the large number of elastomeric bearings, isolation periods ranging from 2.0 to 2.5 sec has been considered and a damping ratio (ξ) equal to 15% has been adopted in order to minimize the base shear transferred to the superstructure. In particular, two cases study have been designed, the first (case 1) characterized by an isolation period of about 2 sec and the second (case 2) characterized by an isolation period of about 2,5 sec. In particular, the isolation system has been designed by following the indications suggested in §7.10.4.2 and C11.9 of the NTC2008 ad by performing a response spectrum analysis at the Collapse Limit State (CLS). More in details, isolation bearings has been designed so that displacements and forces respect the following limitation:

$$\gamma_s \leq \gamma^* / 1{,}5 \leq 2 \tag{1}$$

where γ_s is the shear deformation of rubber layers due to the total seismic displacement (included torsional effects) and γ^* is maximum shear deformation obtained from qualification tests aimed to assess the effective rubber-steel adhesion. The other limitation considered in the design is:

$$\gamma_t = \gamma_c + \gamma_s + \gamma_\alpha \leq 5 \tag{2}$$

where γ_t is the total deformation, γ_c is the shear deformation of rubber layers due to axial load and γ_α is the shear deformation of rubber layers due to angular rotation. Additionally, for the critical devices it has been checked that the maximum tensile stress is lower than the minimum between $2G_{din}$ and 1 MPa, as stated in §7.10.4.2 of NTC2008, in order to avoid cavitation phenomena. Also the maximum compression acting on the bearings has been checked to be lower than $V_{max,c}/2$, where $V_{max,c}$ is buckling load evaluated as reported in C11.9.7:

$$V_{\max,c} = \frac{G_{din} A_r S_1 D}{t_e} \tag{3}$$

Figure 3a shows the devices configuration for the two study cases considered, with bigger devices placed under the columns with larger axial loads. The HDRB are identified by a two number code, the first number (ϕ) defines the diameter and the second one (t_e) the total rubber layer thickness. Table 1 reports the main design results. In particular, is the isolation period (including the superstructure deformability), T_{is}/T_{bf} is the isolation ratio between the periods of the isolated and base fixed structure, $d_{max,HDRB}$ is the maximum displacement of the bearings leading to the maximum shear strain of the rubber γ_{max}, D/C is the demand/capacity ratio in terms of shear strain (D/C shear), vertical compression load (D/C compr), vertical tensile stress (D/C tens) and inter-story drift at Damage Limit State (D/C drift DLS). For the hybrid (elastomeric + steel/PTFE sliders) isolation system the devices configuration examined is illustrated in Figure 3b. It is worth noting that a number of sliders equal to 1/3 of the total devices has been assumed to ensure an appropriate horizontal rigidity. In this case, in order to cover typical situ-

ations that can be found in the current practice, a certain number of isolation systems, characterized by damping ratio equal to 10 or 15% and isolation period ranging from 2.5 to 3.0 sec, have been considered. The design of the isolation bearings has been conducted according to the limitations illustrated for the cases study presenting an isolation system composed only by HDRBs. The characteristics of the four case studies (superstructure + isolation system), as well as the main design results, are reported in Table 2.

Finally, the design of the isolation system based on FPS has been performed to reach higher isolation periods [3]. In particular, two different cases are designed: the first one (case 1) with lower isolation period (effective radius R_e=3100mm corresponding to an isolation period of T_{is}=3.5sec) and higher energy dissipation (medium friction); the second one (case 2) with higher isolation period (effective radius R_e=3700mm corresponding to an isolation period of T_{is}=3.9sec) and lower energy dissipation (low friction). Preliminary design has been completed trough an equivalent linear response spectrum analysis in order to define the design displacement d_{dc} of the isolation system. Design value is calculated at Collapse Limit State (CLS) with an iterative procedure, as described in § 7.10.5.2 of NTC2008, because the isolation system properties are dependent from the design displacement value. To determine the effective stiffness K_e, the effective period T_e and effective damping ξ_e of the equivalent linear model, the following expressions have been used:

$$K_e = N\left(\frac{1}{R_e} + \frac{\mu}{d_{dc}}\right) \qquad T_e = \pi\sqrt{\frac{1}{g\left(\frac{1}{R_e} + \frac{\mu}{d_{dc}}\right)}} \qquad \xi_e = \frac{2}{\pi}\cdot\frac{1}{\frac{d_{dc}}{\mu \cdot R_e} + 1} \qquad (4\ \text{a,b,c})$$

where N is the actual vertical load, R_e is the effective radius, μ is the friction coefficient, g is the gravity acceleration. On the base of suppliers' data, the characteristics of the isolators, in terms of displacement capacity d_m, have been selected and compared with design values of the two case studies. Table 3 shows the characteristics of the FPS systems. In terms of vertical load capacity, 2 different model have been selected for external and internal bearings, in order to ensure the ratio $N_{Sd}/N_{Ed} > 0.5$, where N_{Sd} is maximum vertical load capacity in static conditions and N_{Ed} is the maximum vertical load capacity in dynamic conditions (Figure 3c).

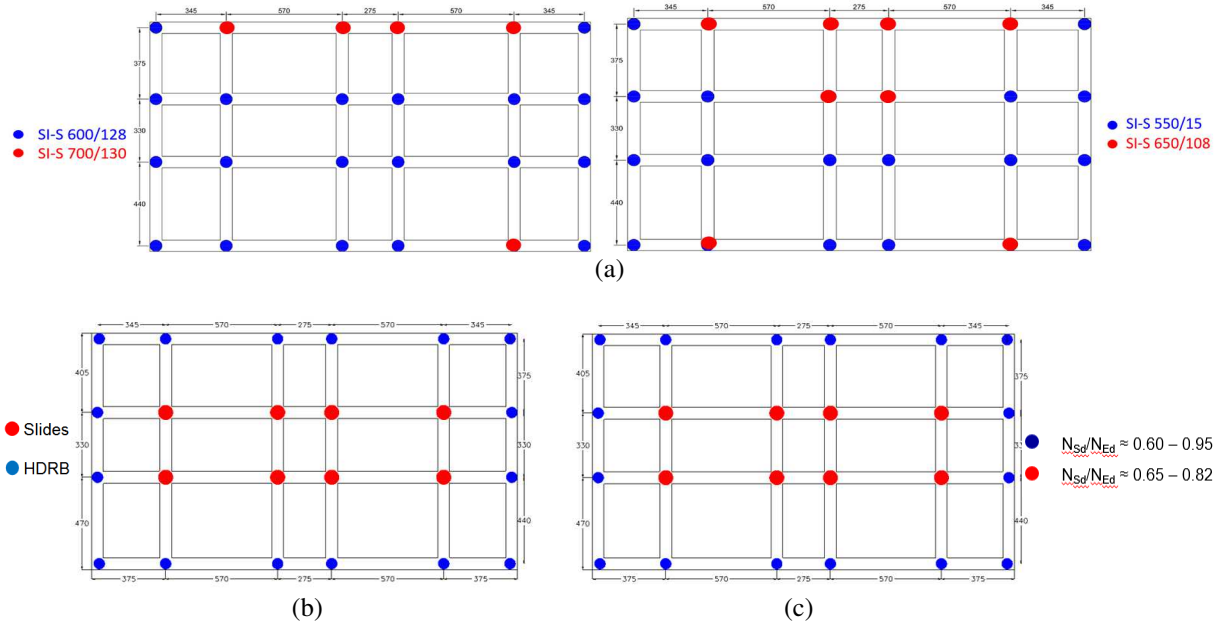

Figure 3: isolation system configuration of a) HDRBs, b) hybrid case and c) FPS

CASE	HDRB ϕ/t_e	ξ [%]	$d_{max,HDRB}$ [mm]	T_{is} [s]	γ_{max}	D/C shear	D/C compr.	D/C tens.	T_{is}/T_{bf}	D/C drift DSL
case 1	600/128 + 700/130	15	250	2,04	1,63	0,82	0,82	0,99	2,60	0.31
case 2	550/154 + 600/150	15	300	2,46	1,71	0,86	0,97	0,33	3,46	0.21

Table 1: geometric characteristics and design outcomes for HDRB isolation system

CASE	HDRB ϕ/t_e	SLIDES $V/d_{max,x}/d_{max,y}$	ξ [%]	d_{max} [mm] HDRB	d_{max} [mm] Slides	T_{is} [s]	γ_{max}	D/C shear	D/C compr.	D/C tens.	T_{is}/T_{bf}	D/C drift DSL
case 1	650/180	350/700/700	10	350	350	2.84	1.83	0.94	0.89	0.83	3.05	0.36
case 2	600/152	350/600/600	15	300	300	2.84	1.88	0.95	0.82	0.54	3.05	0.30
case 3	600/176	350/700/700	15	350	350	3.04	1.7	0.85	0.98	0.19	3.27	0.27
case 4	700/180	350/700/700	10	350	350	2.66	1.69	0.87	0.65	0.94	2.86	0.30

Table 2: geometric characteristics and design outcomes for hybrid isolation system

CASE	R_e [mm]	μ [%]	d_{dc} [mm]	d_m [mm]	$T_e(d_{dc})$ [sec]	$\xi_e(d_{dc})$ [%]
case 1	3100	5.50	168	± 250	2.49	32
case 2	3700	2.50	258	± 300	3.37	17

Table 3: geometric characteristics and design outcomes for FPs isolation system

2.2 Superstructure

According to NTC 2008, the Life Safety Limit State has been assumed as reference for the structural design. All buildings were designed using the Response Spectrum Analysis, neglecting capacity design while considering low ductility class (CDB) for structural details. The superstructure is classified as ordinary, thus the importance factor is Cu=1. The staircase is part of the building structure and has been designed using knee beams. A supplementary floor has been added at the bottom of the first storey columns and a grid of RC beams has been implemented at the aforesaid level of the building. It is commonplace in Italy to use masonry infills in the building outer walls. As a consequence, regularly distributed infill panels, in plan and elevation, have been considered. Infills are not included as structural elements in the building model but are only included as dead loads. For each isolation typology, the case study that maximizes the base shear transferred to the superstructure has been used for the structural design of the building. Table 4 summarizes the design data of the selected prototypes for the study cases. In particular, $\Sigma A_{col}/A_{floor}$ is the total column area at the ground floor divided the total floor area; $\rho_{b\_deep,1,m}$ is the average deep beams' longitudinal steel ratio, $\rho_{b\_flat,1,m}$ is the average flat beams' longitudinal steel ratio and $\rho_{c,1,m}$ is the average base floor columns' steel ratio.

	Average floor [kN/m^2]	$\Sigma A_{col}/A_{floor}$ [%]	$\rho_{b\_deep,1,m}$ [%]	$\rho_{b\_flat,1,m}$ [%]	$\rho_{c,1,m}$ [%]
HDRB	13.1	1.80	1.0	1.1	1.13
HDRB-FSB	12.6	1.81	1.1	1.0	0.9
FPS	14.7	1.77	0.8	0.8	0.9

Table 4: global load and reinforcement characteristics

The column area and the reinforcement ratio are almost the same for all the study cases. In fact, the column sizes mainly derive from pre-sizing based on the assumed maximum normalized axial load and in most cases the amount of reinforcement is given by the minimum reinforcement requirements of NTC 2008. The staircase knee beams experience high tension/compression excursions, pointing to possible numerical issues in the nonlinear analyses.

3 MODELLING STRATEGIES

A nonlinear model of the all cases study has been developed in the computational platform OpenSees [4], including the superstructure and the isolation system. In particular, for the isolation devices accurate nonlinear models have been selected in order to correctly predict the response of the isolated building. On the contrary, in the superstructure modelling pragmatic choices have been done due to the size of the building and the number of analyses to be carried out. In this section, a description of the adopted models is reported for both the isolation system and the superstructure.

3.1 Isolation system

To describe the cyclic behavior of the HDRBs, the selected model is that recently developed by Kumar et al. 2014 [5] and implemented in Opensees as HDR Bearing Element. The physical model is as a two-node, twelve degrees-of-freedom discrete element. The two nodes are connected by six springs that represent the mechanical behavior in the six basic directions of a bearing. The coupling of the two shear springs is considered directly by using a coupled bidirectional model. All other springs are uncoupled. The coupling of vertical and horizontal directions are partially considered (in an indirect way) by using expressions for mechanical properties in the vertical direction that are dependent on the response parameters in the horizontal direction (but properties in the horizontal direction does not depend on the response in the vertical direction in the current version of the model). Linear uncoupled springs are considered in the torsion and the two rotational springs, as they are not expected to significantly affect the response of an elastomeric bearing. The material model in the axial direction (Figure 4) is based on a mathematical model developed by Kumar [5] that captures the cavitation and post-cavitation behavior in tension and the variation of the critical buckling load and the vertical axial stiffness with horizontal displacement in compression. The bidirectional model proposed by Grant et al. 2004 [6] is adopted to describe the behavior under the two shear directions (Figure 5). This model is able to capture the degradation of bearing stiffness and damping due to scragging effects in shear, which is of particular importance for high dissipative rubbers [6][7]. For the torsional behavior in the two rotational directions, a linear elastic model is assumed.

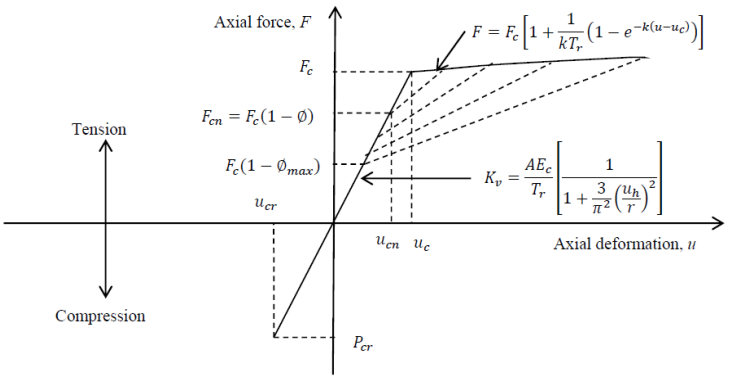

Figure 4: global mathematical model of elastomeric bearings in axial direction

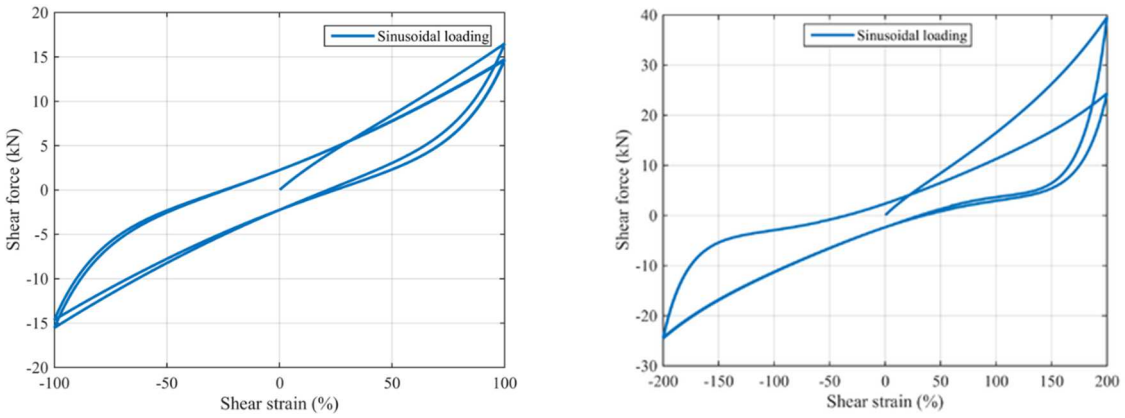

Figure 5: global mathematical model of elastomeric bearings in shear accounting for the stress softening

An iterative procedure has been followed to calibrate the model parameters, based on the fitting of experimental tests carried out on real scale HDRBs (provided by the university of Basilicata) made by a soft rubber with shear modulus G=0.4 MPa. Figure 6 shows the comparison between the calibrated model (blue line) and the experimental data (red line) in terms of shear stress-strain relation. The first test (Figure 6a) has been carried out up a shear deformation equal to 1.5 on the virgin device, whereas the second one (Figure 6b) is the repetition of the first test on the same devices after a series of tests at strains larger than 1.5 (scragged device). In Figure 7a three tests carried out up to a maximum strain of 3.8 are reported with the numerical simulation (blue line). The test depicted with the yellow line has not been considered for the calibration because the failure of the device connection has occurred. Since the equivalent linear parameters at the third cycle of the bearing rubber used for the experimental tests are G = 0.37 and ξ = 0.137, the obtained model parameters have been modified in order to obtain the design value. In particular the model parameter used to simulate the rubber with equivalent linear parameters G = 0.4 and ξ = 0.15 are reported in the first row of Table 5. In the second row the parameters used to simulate the less dissipative rubber used in the design (G = 0.4 and ξ = 0.10) are reported. The differences between the two design rubbers are illustrated by the hysteresis loops reported in Figure 7b.

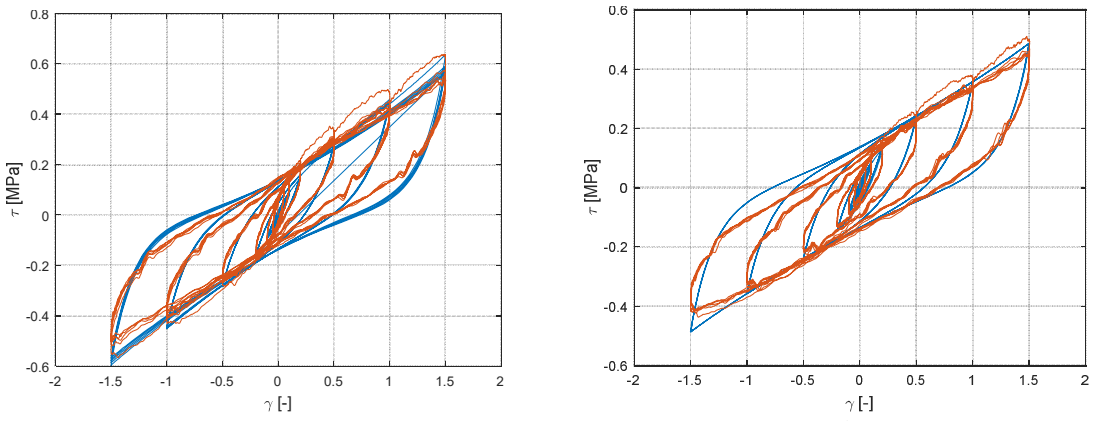

(a) (b)

Figure 6: cyclic shear test on the a) virgin and b) scragged device

Actually Grant model [6] has 10 parameters which define the behaviour of the entire bearing (a_1, a_2, a_3 for the elastic component, b_1, b_2, b_3 for the inelastic component, c_1, c_2, c_3, c_4 for the damage). Thus, a procedure to convert rubber parameters to bearing parameters has been developed, by implementing the following relations, where A is the rubber area and T_r is the total rubber thickness:

$$a_1 = \alpha_1 \cdot A / T_r \qquad a_2 = \alpha_2 \cdot A / T_r^3 \qquad a_3 = \alpha_3 \cdot A / T_r^5 \qquad (5\ a,b,c)$$

$$b_1 = \beta_1 \cdot A \qquad b_2 = \beta_2 \cdot A / T_r^2 \qquad b_2 = \beta_2 / T_r \qquad (6\ a,b,c)$$

$$c_1 = \chi_1 / T_r^3 \qquad c_2 = \chi_2 / T_r^3 \qquad c_3 = \chi_3 \qquad c_4 = \chi_4 / T_r^3 \qquad (7\ a,b,c)$$

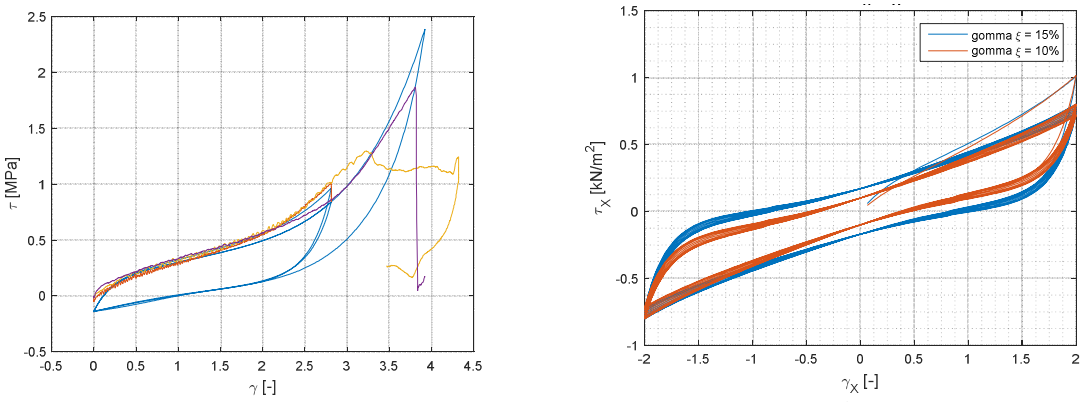

(a) (b)

Figure 7: a) shear tests up to large strains and b) comparison between the two design rubbers

Rubber	α_1	α_2	α_3	β_1	β_2	β_3	χ_1	χ_2	χ_3	χ_4
ξ=0.15	276.03	17.19	3.606	170.37	77.106	5.094	0.01287	0.086	0.8306	0.00005
ξ=0.10	314.94	17.19	3.606	100.22	77.106	5.094	0.01287	0.086	0.8306	0.00005

Table 5: model parameters for the shear behaviour of HNDR bearings

The nonlinear behaviour of the FPSs has been modelled by using one joint link element type biaxial Friction-Pendulum Isolator. The friction and pendulum forces are directly proportional to the compressive axial force in the element which cannot carry axial tension [8]. The cyclic nonlinear behaviour is expressed through the initial stiffness K_i (before sliding, with a quasi-rigid behaviour), and the restoring stiffness $K_r=N/R_e$, as shown in Figure 8. The velocity dependence of the friction coefficient is described by the Constantinou et al. [9] model:

$$\mu = \mu_{fast} - \left(\mu_{fast} - \mu_{slow}\right) \cdot e^{-\alpha|v|} \qquad (8)$$

where v is the sliding velocity; μ_{fast} and μ_{slow} are the sliding coefficients of friction at maximum and minimum velocity respectively; α is a rate parameter that controls the transition from μ_{slow} to μ_{fast}. The axial load dependence of the coefficient of friction is not considered in this study.

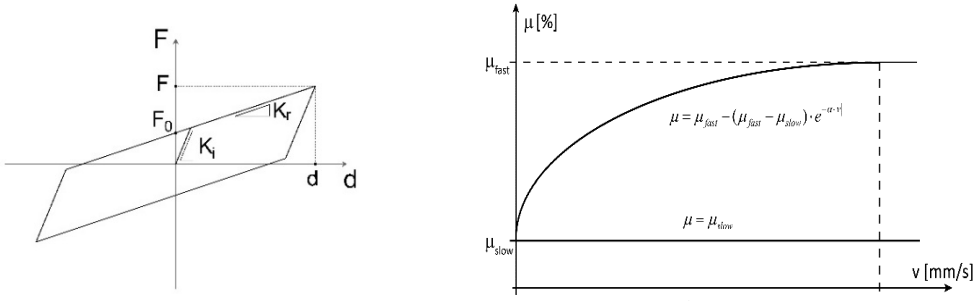

(a) (b)

Figure 8: a) nonlinear cyclic behaviour of the DCFP bearings and b) velocity dependent friction model.

Table 6 reports the main parameters of the FPS numerical model. For each case study, the values of μ_{slow} is the friction coefficient as declared by the manufacturer. The other parameters

(μ_{fast}, α and K_i) have been calibrated on the base of experimental characterization tests on similar bearings. Large values have been used for vertical stiffness, K_V.

Case	Radius (mm)	μ_{slow} (%)	μ_{fast} (%)	α (s/m)	K_i (kN/m)	K_V (kN/m)
Case 1	3100	5.5	8.0	5.0	5000	1E^10
Case 2	3700	2.5	5.0	5.0	5000	1E^10

Table 6: FPS model parameters

3.2 Superstructure

A lumped plasticity model has been chosen for beam and column members of the superstructure, whereas elastic beams have been used for the base floor grid above the isolation system. The choice of representing the superstructure with a nonlinear model is justified by the results of recent studies on this topic [10], which pointed out the effects of the inelastic behaviour of the superstructure on the seismic response of base isolated structures. The model also includes the staircase structure (inclined beams and cantilever steps) as well as masonry infill panels. In particular, in order to limit the forces acting on the inclined beams to values compatible with their strength, the stiffness of the axial degree of freedom of the internal elastic element has been reduced to zero, while putting an inelastic truss element in parallel with a non-symmetric elastic plastic constitutive law. The contribution of the masonry infill panel to the response of the reinforced concrete frame is modelled by replacing the panel with an equivalent strut acting only in compression. The equivalent diagonal strut is a coherent engineering model for infilled frames and a modified version of Decanini et al. model [11] was selected for modelling the struts. The effects of the openings were accounted for through reduction factors [12] according to Figure 9.Considering that the modelling choices concerning the structural (and non-structural) elements of the superstructure have been derived from those adopted by WP working on RC frames, reference to [2] can be made for all the modelling details.

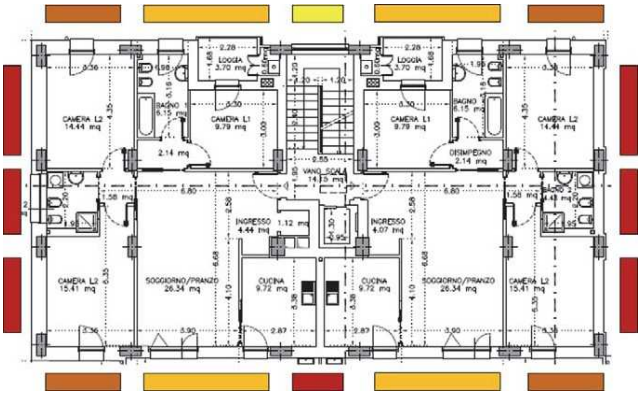

Figure 9: masonry infill panels: percentage of openings (from 100% yellow to 0% red)

4 NONLINEAR DYNAMIC TIME HISTORY ANALYSES

The seismic vulnerability of the designed structures was assessed by means of multi-stripe non-linear dynamic analysis carried out by considering 10 intensity levels with 20 ground motions per stripe. For base isolated buildings, the collapse condition could be related to the collapse of the superstructure or the collapse of the isolation system, which are both described in this section. The collapse of the structural system is deemed attained when the collapse of one of components of the structural system is reached.

4.1 Isolation system collapse conditions

The global collapse condition of the isolation system depends on the typology and the associated failure modes of the specific devices composing the system. For what concerns HDRBs, in the present study the collapse of a singular elastomeric device has been associated to the occurrence of one of the following failure modes: i) cavitation ii) buckling iii) shear. About the first failure mode, recent experimental tests have shown that elastomeric bearings can sustain large tensile strains of up to 100% following cavitation, without rupture of the bearing [13]. In this work an axial tensile strain equal to 0.5 has been prudently assumed as reference threshold and the global collapse condition has been conventionally fixed when the 50% of elastomeric devices reaches an axial tensile strain greater or equal to the assumed threshold. For the buckling failure, a step-by-step value of the critical buckling load of each device have been recorded during the analyses in the Opensees environment. Therefore, the P/P_{cr} ratio between the current axial load and the critical buckling load has been evaluated in order to identify the collapsed devices i.e. when $P/P_{cr}=1$. The global collapse condition has been conventionally fixed when the 50% of elastomeric devices simultaneously reaches a value of the axial compressive force equal to the critical buckling load. Finally, with regard to the shear failure, recent studies [14] pointed out a lower bound limit for rubber failure in terms of shear deformation (γ) of about 260%, regardless the shape factor value and the applied pressure. Such value seems to be excessively precautionary if compared to the experimental results obtained by Muramatsu et al. [15] and Kawamata and Nagai [16], which propose values of the order of 400-500%. All that considered, a limit value equal to 350% has been assumed in the present study, which also corresponds to the maximum shear strain of the experimental tests used to calibrate the horizontal shear behaviour of the numerical HDR model. The global collapse condition has been conventionally fixed when the 50% of elastomeric devices reaches a shear strain greater or equal to the assumed limit.

For what concerns the steel/PTFE sliders, the failure has been associated to a horizontal displacement value equal to the device capacity increased by an extra-displacement equal to the bearing radius. The current displacement of centre of gravity of the base floor has been assumed as displacement demand. Similarly, the collapse of a singular FP device is associated to a horizontal displacement value equal to the maximum displacement capacity d_m increased by an extra-displacement capacity (+10% of d_m). The current displacement at the external angle joint of the base floor has been assumed as displacement demand. All the collapse conditions are summarized in Table 7. Obviously in the case of HDRBs or hybrid systems, the collapse of the isolation system is deemed attained when one of the associated collapse conditions is reached.

FAILURE MODE	COLLAPSE CONDITIONS	
Buckling	50% of elastomeric devices (simultaneously) reaches a value of the axial compressive force equal to the critical buckling load;	$P/P_{cr}=1$
Cavitation	50% of elastomeric devices reaches an axial tensile strain (ε_t) greater or equal to 50%;	$\varepsilon_t \geq 50\%$
Shear	50% of elastomeric devices reaches a shear strain (γ) greater or equal to 3.5;	$\gamma \geq 3.5$
Sliders	The center of gravity of the base floor reaches an horizontal displacement equal to the device capacity increased by an extra-displacement.	$d_u = d_{max,slide}+\phi/2$
FPS	The external angle of the base floor reaches an horizontal displacement equal to the device capacity increased by an extra-displacement.	$d_u = 1.1 d_{max,FPS}$

Table 7: collapse Conditions for the isolation system

4.2 Superstructure collapse condition

For the superstructure, an approximate criterion is adopted. In fact, capacity is defined as the value of drift (IDR or RDR can be used indifferently for these buildings) at 50% decrease in base shear on the negative slope. This value is preferred since it is easier to identify on the pushover curves. Obviously, the fixed base configuration has been considered to perform the pushover analysis of the examined building. Two values of collapse are determined, one in the X and the other in the Y direction (single value, no significant difference was detected between '+' and '-').All the push over curves are reported in Figure 10.

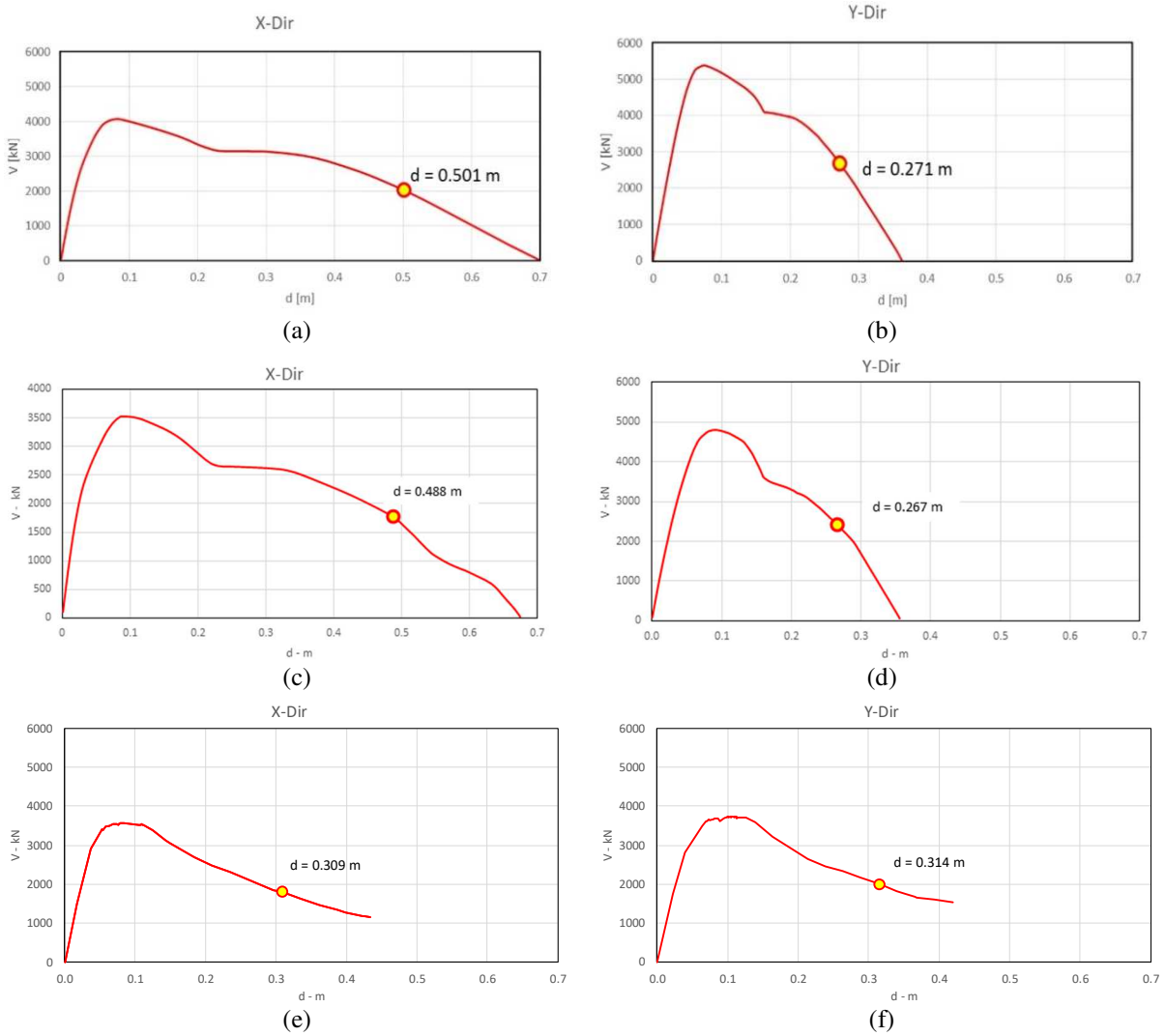

Figure 10: pushover curves and displacement thresholds in the X and Y-directions at CLS for a-b) HDRB, c-d) HDRB+FSB and e-f) FPS (without infills).

4.3 Results of nonlinear dynamic time history analyses at the Collapse Limit State

The analyses results for the Collapse Limit State are summarized in this section in terms of number of failures. In other words, the total number of records determining a collapse condition for the base isolated building is reported as a function of the seismic intensity. Moreover, the failure modes that caused the collapse are pointed out for each record by using different colours. The results presented in Figure 11 are related to the cases study presenting an isolation system composed only by HDRBs and point out that, for an intensity measure level corresponding to

a return period equal to 1000 years (i.e. IM6), typically assumed as Collapse Limit State according to NTC2008, no failures are recorded. As a general trend, a significant number of failures is recorded above IM 9. Such failures are mainly associated to the superstructure in the case 1, due to the lower value of the isolation ratio. Differently, in the case 2, characterized by a lower margin with respect to the buckling load capacity, the failures are associated to both the superstructure and buckling of bearings. For the sake of completeness, a comparison between the results obtained for case 2 using two different set of ground motions, with conditioning period 2.0 and 3.0 seconds, is presented in Figure 12. In the case 2b a significant number of failures is recorded above IM 7. The difference between the obtained results is due to the different characteristics of the records included in the two set. More detail can be found in [17] which is the paper of the WP working on the seismic input and risk assessment procedure.

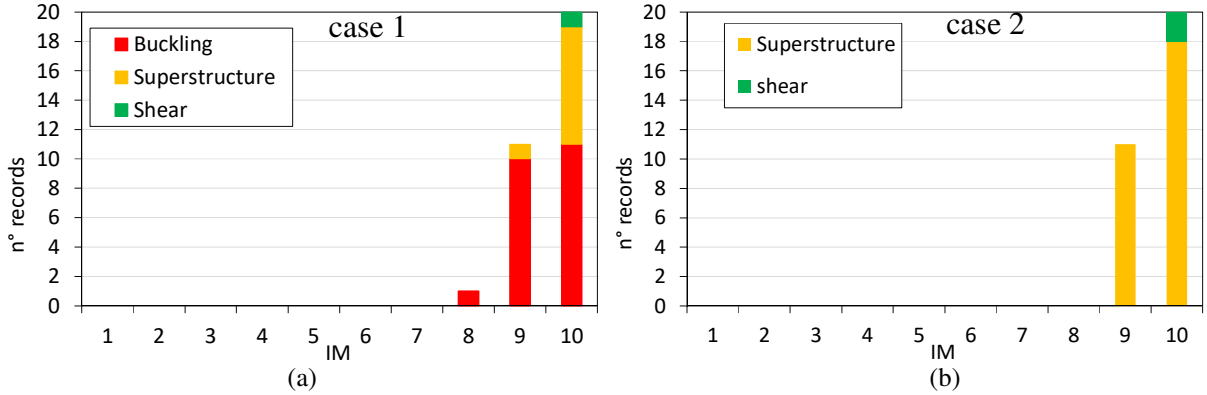

Figure 11: summary of NTHAs' results at CLS for a) case 1 and b) case 2 for HDRB

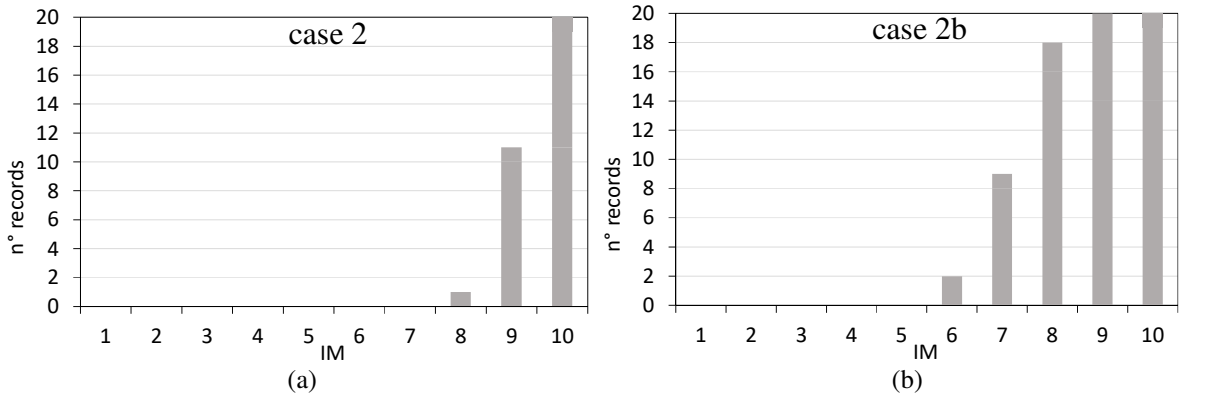

Figure 12: NTHAs' results at CLS for HDRB case 2 obtained using a) conditioning period equal to 2 sec and b) conditioning period equal to 3 sec.

The results presented in Figure 13 are related to the four cases study presenting an hybrid system. Also in this case, the obtained results point out that, for the intensity measure level corresponding the Collapse Limit State (i.e. IM6) no failures are recorded, whereas a significant number of failures is recorded above IM 7. Such failures are mainly associated to buckling phenomenon except for case 4. For the latter, as expected, the superstructure collapse is the prevalent failure mode due to a lower value of the isolation ratio.

Finally, results presented in Figure 13 are related to the cases study with FP devices. Also in this case, no failures are recorded at IM6, whereas a significant number of failures is recorded above IM 7 for the isolation system and between IM8/IM9 for the superstructure.

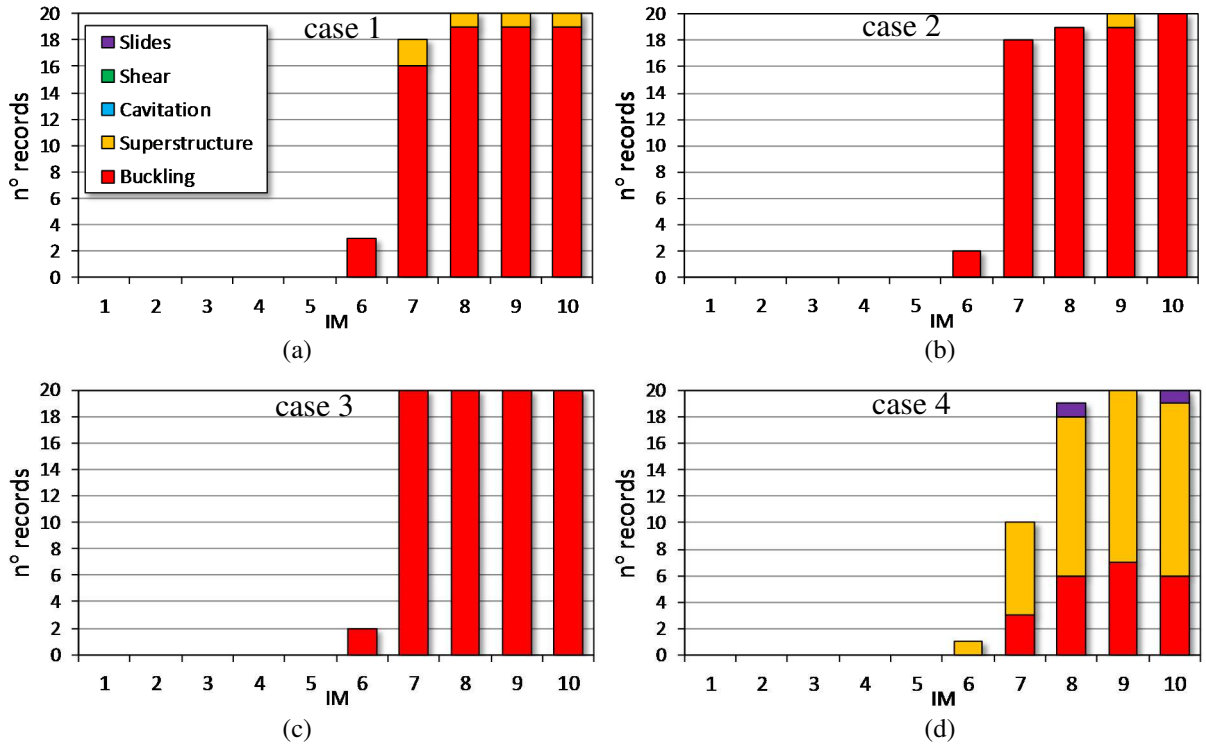

Figure 13: summary of NTHAs' results at CLS for a) case 1, b) case 2, c) case 3 and d) case 4 for HDRB+FSB RU

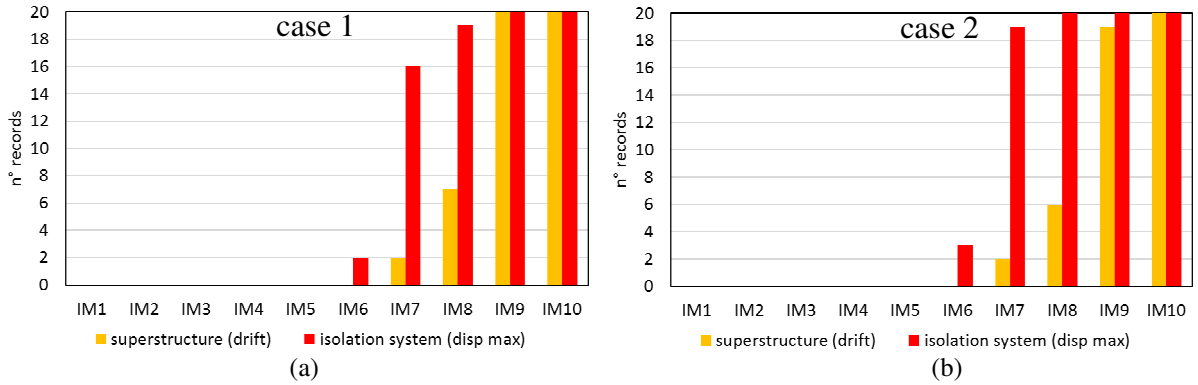

Figure 14: summary of NTHAs' results at CLS for a) case 1 and b) case 2 for FPS

Based on the results obtained, limited safety margins with respect to the collapse of the building have been observed, for all the isolation systems considered and for almost all the study cases analysed. This is due to an optimized and controlled design of the isolation system towards the above mentioned limit state.

4.4 Results of nonlinear dynamic time history analyses at the Damage Limit State

The Damage Limit State is defined in NTC2008 as the limit state where "*the structure, including structural and nonstructural elements, and machines relevant to its functions, exhibit damage that does not expose its occupants to any risk, and that does not compromise the strength and stiffness of the structure with respect of the vertical and horizontal loads. The structure is immediately usable even if some machineries are not fully operational.*" Based on the above definitions, Italian design guidelines define InterStory Drift Ratios (IDRs) limits for existing buildings equal to IDR $\leq$ 0.003, if the model includes the infills, and IDR $\leq$ 0.005 for the Bare Frame case. Thus, in the present study, the failure condition has been assessed by

comparing the Demand inter-storey drift (i.e. the maximum inter-storey drift value derived from Non Linear Time History Analyses), with the Capacity inter-storey assumed equal to 3‰. In this optic, D/C ratios larger than 1 are associated to the mentioned failure condition.

The analyses results for the Damage Limit State are summarized in this section in terms of D/C ratios (where D represents the largest IDR over X and Y directions of top displacement demand-absolute value) associated to each singular record and IM for each case study. In particular D/C ratios for the study cases are reported in Figure 15, Figure 16 and Figure 17.

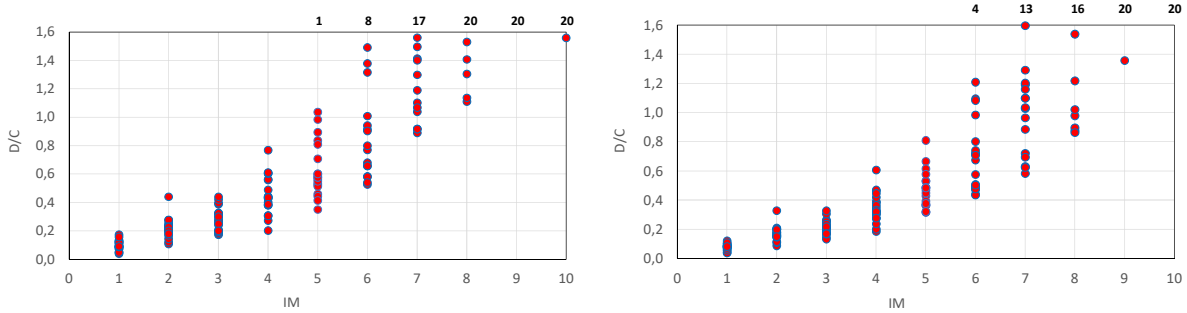

(a) (b)

Figure 15: D/C ratios for a) case 1 and b) case 2 for HDRB

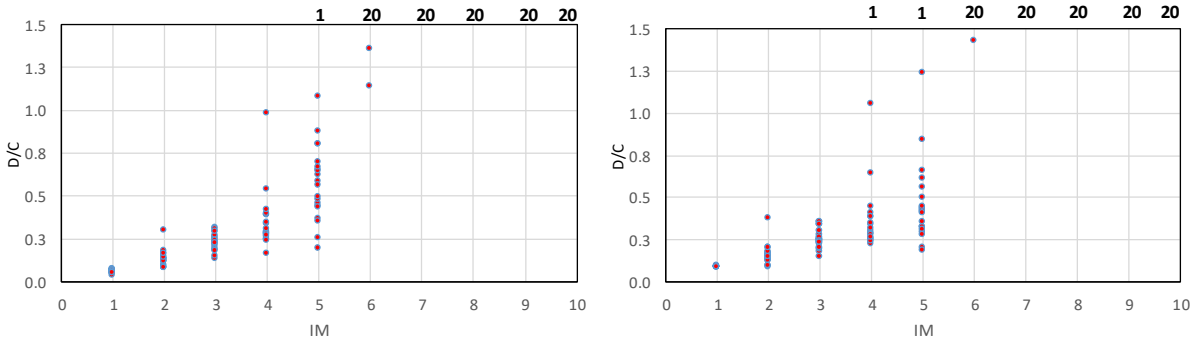

(a) (b)

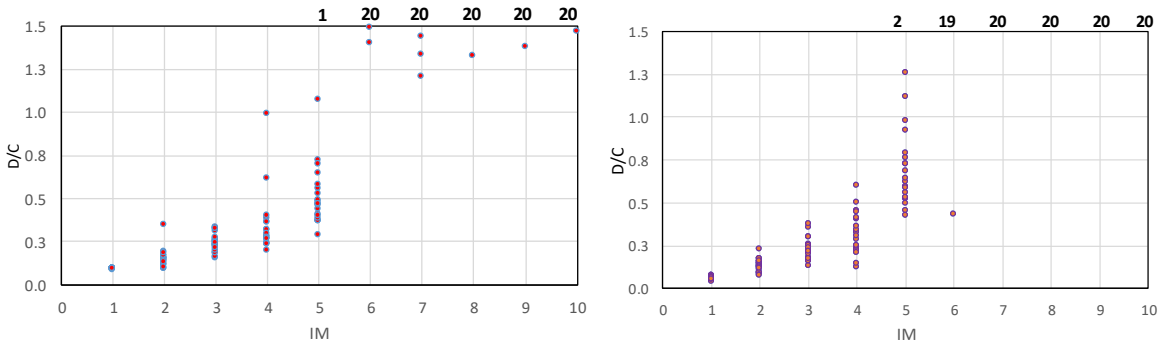

(c) (d)

Figure 16: D/C ratios for a) case 1, b) case 2, c) case 3 and d) case 4 for HDRB+FSB

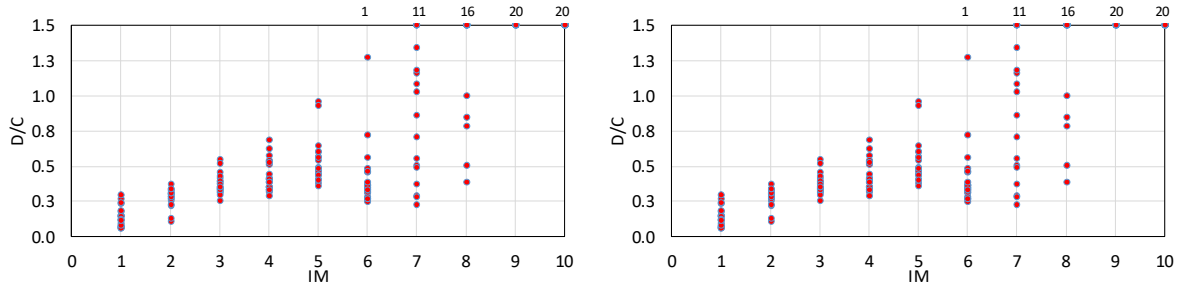

(a) (b)

Figure 17: D/C ratios for a) case 1 and b) case 2 for FPS.

Al the results presented point out that, for an intensity measure level corresponding to a return period equal to 50 years (i.e. IM2), typically assumed as Damage Limit State according to NTC2008, no failures are recorded and D/C ratios sensibly lower than 1 are obtained. A significant number of failures (D/C≥1) is obtained only for seismic events characterized by return periods greater than 1000 years (i.e. IM6). Based on the results obtained at DLS, a large margin with respect to the capacity of the building at the DLS have been observed, for all the isolation systems considered and for almost all the study cases analyzed. This is due to the high protection level that seismic isolation techniques are able to provide against the attainment of the DLS, which has been resulted much greater that for fixed-base buildings.

5 CONCLUSIONS

This paper presents the results of an ongoing project on the implicit risk of seismic collapse (and damage) of isolated buildings designed according to the current Italian design code NTC2008. The paper focuses on a six storey RC building isolated with different base seismic isolation systems based on: (i) rubber bearings, (ii) rubber bearings and flat sliding bearings, (iii) friction pendulum systems. The design procedure of the isolation system and the superstructure, according to current Italian seismic code, has been shown, and a nonlinear model of the all cases study has been developed in the computational platform OpenSees, using available advanced elements for the isolators' behaviour. Definitions of collapse and damage limit states are discussed. Finally, the failure conditions of the proposed isolation systems and peak responses of building have been evaluated through nonlinear dynamic analysis performed under bidirectional ground motions considering twenty couple of natural earthquakes for ten different peak ground accelerations. The results point out that all isolation systems work effectively in limiting the building damage for seismic intensities much higher than the design earthquake. On the other hand, they have a little margin to collapse beyond the design seismic intensity.

ACKNOWLEDGEMENTS

The authors would like to acknowledge the financial support of the Italian Civil Protecction Department, ReLUIS project 2014-2018 (http://www.reluis.it/).

REFERENCES

[1] NTC 2008, *Norme Tecniche per le Costruzioni*, Decreto ministeriale del 14 gennaio 2008, in Italian (Italian Building Code, 2008).

[2] Camata G., Celano F., De Risi M., Franchin P., Magliulo G., Manfredi V., Masi A., Mollaioli F., Noto F., Ricci P., Spacone E., Terrenzi M, Verderame G. RINTC project: nonlinear dynamic analyses of italian code-conforming reinforced concrete buildings for risk of collapse assessment. *COMPDYN 2017 - 6th ECCOMAS Thematic Conference on Computational Methods in Structural Dynamics and Earthquake Engineering* M. Papadrakakis, M. Fragiadakis (eds.) Rhodes Island, Greece, 15–17 June 2017.

[3] Ponzo F.C., Di Cesare A., Leccese G., Nigro D. Shaking table tests of a base isolated structure with double concave friction pendulum bearings. *Bulletin of the New Zealand National Society for Earthquake Engineering*, Vol 48, Issue 2, Pages 136–144, 2015.

[4] McKenna F. OpenSees: a framework for earthquake engineering simulation, *Computing in Science & Engineering* 13.4: 58-66, 2011 (http://opensees.berkeley.edu).

[5] Kumar M., Whittaker A. e Constantinou M. An advanced numerical model of elastomeric seismic isolation bearings. *Earthquake Engineering & Structural Dynamics*, 43(13):1955-1974,2014

[6] D. N. Grant , G. L. Fenves e A. Whittaker. Bidirectional modelling of high-damping rubber bearings, *Journal of Earthquake Engineering* 8(1):161-185, 2004.

[7] E. Tubaldi, L. Ragni, A. Dall'Asta, H. Ahmadi, A. Muhr. Stress-softening behaviour of HDNR bearings: modelling and influence on the seismic response of isolated structures, *Earthquake Engineering & Structural Dynamics,* DOI: 10.1002/eqe.2897, 2017.

[8] Di Cesare A., Ponzo F.C., Leccese G., Nigro D. Numerical Modelling of Double Concave Friction Pendulum Bearings in CDS-OpenSees. *OpenSees Days - 2nd Italian Conference*. 10-11 June, Fisciano (SA), Italy. IMREADY s.r.l., 173-180, 2015.

[9] Constantinou BM, Member A, Mokha A, Reinhorn A. Teflon bearings in base isolation. II: modeling. *Journal of Earthquake Engineering*, 116(2), 455–474, 1990.

[10] Cardone D., Flora A., Gesualdi G. Inelastic response of RC frame buildings with seismic isolation*, Earthquake Engineering & Structural Dynamics*, 42:871–889, 2013.

[11] Sassun, K., Sullivan, T. J., Morandi, P., Cardone, D. Characterising the in-plane seismic performance of infill masonry. *Bulletin of the New Zealand Society for Earthquake Engineering*, 49(1): 100-117, 2016.

[12] Cardone, D., Perrone, G. Developing fragility curves and loss functions for masonry infill walls. *Earthquakes and Structures*, 9 (1): 257-279, 2015.

[13] Iwabe N., Takayama M., Kani N., Wada A. Experimental study on the effect of tension for rubber bearings. *Proceedings of the 12th World Conference on Earthquake engineering*, New Zeland, 2000

[14] G. M. Montuori, E. Mele, G. Marrazzo, G. Brandonisio, A. De Luca. Stability issues and pressure–shear interaction in elastomeric bearings: the primary role of the secondary shape factor. *Bulletin of Earthquake Engeneering,* 14:569–597, 2016.

[15] Muramatsu, Y., Inoue, K., Katoh, R., Kamitani, N., Sakaguchi, T., Sasaki, Y., Kitamura, H. Test results of ultimate properties of rubber bearings for buildings. *AIJ J Technol Des*, (20): 67-70, 2004.

[16] Kawamata, S., and K. Nagai. "Ultimate deformation capacity of isolators." *International workshop on recent developments in base-isolation techniques for buildings*, Tokyo. 1992.

[17] I. Iervolino, A. Spillatura, P. Bazzurro. RINTC Project - Assessing the (implicit) seismic risk of code-conforming structures in Italy. *COMPDYN 2017 - 6th ECCOMAS Thematic Conference on Computational Methods in Structural Dynamics and Earthquake Engineering*, M. Papadrakakis, M. Fragiadakis (eds.) Rhodes Island, Greece, 15–17 June 2017.